

SPT: Fine-Tuning Transformer-based Language Models Efficiently with Sparsification

Yuntao Gui

The Chinese University of Hong Kong
Hong Kong SAR, China
yogui@cse.cuhk.edu.hk

Xiao Yan

Southern University of Science and
Technology
China
yanx@sustech.edu.cn

Peiqi Yin

The Chinese University of Hong Kong
Hong Kong SAR, China
pqyin22@cse.cuhk.edu.hk

Han Yang

The Chinese University of Hong Kong
Hong Kong SAR, China
hyang@cse.cuhk.edu.hk

James Cheng

The Chinese University of Hong Kong
Hong Kong SAR, China
jcheng@cse.cuhk.edu.hk

ABSTRACT

Transformer-based large language models (e.g., BERT and GPT) achieve great success, and *fine-tuning*, which tunes a pre-trained model on a task-specific dataset, is the standard practice to utilize these models for downstream tasks. However, Transformer fine-tuning has *long running time* and *high memory consumption* due to the large size of the models. We propose the SPT system to fine-tune Transformer-based models efficiently by introducing *sparsity*. We observe that the memory consumption of Transformer mainly comes from storing attention weights for multi-head attention (MHA), and the majority of running time is spent on feed-forward network (FFN). Thus, we design the *sparse MHA* module, which computes and stores only large attention weights to reduce memory consumption, and the *routed FFN* module, which dynamically activates a subset of model parameters for each token to reduce computation cost. We implement SPT on PyTorch and customize CUDA kernels to run sparse MHA and routed FFN efficiently. Specifically, we use product quantization to identify the large attention weights and compute attention via sparse matrix multiplication for sparse MHA. For routed FFN, we batch the tokens according to their activated model parameters for efficient computation. We conduct extensive experiments to evaluate SPT on various model configurations. The results show that SPT consistently outperforms well-optimized baselines, reducing the peak memory consumption by up to 50% and accelerating fine-tuning by up to 2.2 \times .

KEYWORDS

language models, transformer, model training, fine-tuning

1 INTRODUCTION

Recently, large language models (e.g., BERT [11], RoBERTa [25], GPT-2 [30], OPT [46], and LLaMa [40]) show amazing performance for many tasks such as machine translation, text generation, and question answering. However, training these models from scratch is prohibitively expensive, requiring enormous general-purpose corpus and millions of GPU hours [7, 28], which are beyond reach for most practitioners. As such, *fine-tuning* has become the standard practice to utilize these models for downstream tasks [17, 18, 37, 44]. In particular, fine-tuning takes a pre-trained model, whose

Table 1: Time and memory decomposition for a Transformer block (see § 6 for settings). Full is full-parameter tuning, and LoRA is low-rank adaption. Total peak memory is smaller than summation due to dynamic tensor destruction.

	Running Time			Peak Memory		
	MHA	FFN	Total	MHA	FFN	Total
Full	59.6 ms	128.8 ms	188.4 ms	3.2 GB	1.3 GB	3.2 GB
LoRA	52.5 ms	108.5 ms	161.0 ms	2.6 GB	1.1 GB	2.7 GB
SPT	54.1 ms	54.9 ms	106.0 ms	0.9 GB	1.1 GB	1.6 GB

parameters encompass rich knowledge learned from a general-purpose corpus, and continues to train the model on a task-specific dataset, which is usually much smaller. It has been shown that fine-tuning yields good model quality for various tasks [5, 36, 41, 45] while significantly reducing the cost of end-to-end training [4, 17, 37].

However, fine-tuning is still reasonably expensive given the large size of the language models, and many methods are proposed to improve efficiency such as BitFit [44], Input-Tuning [1], and LoRA [18]. Among these methods, *low-rank adaptation* (LoRA) is popular, which freezes the pre-trained model parameters and introduces a small number of new parameters to update during fine-tuning. Specifically, LoRA uses small low-rank matrices as the new model parameters to reduce the number of parameters to update and is widely used due to its good model quality and efficiency [12, 24]. For instance, Table 1 shows that LoRA reduces both running time and memory consumption compared with full-parameter tuning that updates all the original model parameters. Note that besides running time, memory consumption is also important for fine-tuning as the memory requirement scales with sequence length for language models, reduced memory consumption allows the models to be trained on a wider variety of downstream tasks (e.g., chatbot and text summarization).

Although LoRA already outperforms full-parameter tuning, we ask the following research problem—*can the efficiency of LoRA be improved further?* To explore the opportunities for improvement, we profile the costs of a Transformer block in Table 1. Transformer

is the basic building unit of large language models, and most models can be viewed as stacking multiple Transformer blocks. In a Transformer block, there are two main modules, i.e., *multi-head attention* (MHA) and *feed-forward network* (FFN). MHA allows the tokens in a sequence to attend to each other to capture context, while FFN transforms the token embeddings by matrix mapping. The results in Table 1 show that for both full-parameter tuning and LoRA, the main memory consumption is caused by MHA while the majority of running time is spent on FFN.

Motivated by the observations above, we build the SPT system to conduct LoRA fine-tuning efficiently by exposing sparsity in the two key modules of Transformer. In particular, we find that MHA takes huge memory to store the attention weights between all token pairs, and propose the *sparse MHA*, which keeps only the top- L attention weights for each token. This does not harm model quality because the attention weights are generated by softmax, and thus the top- L weights dominate the total weights and yield a small approximation error. The FFN is computationally expensive because its projection matrices are large with many parameters. We propose the *routed FFN*, which organizes the parameters in blocks and dynamically determines the parameter blocks to activate for each token. Routed FFN reduces computation as each token now uses only some of the parameters.

We implement SPT on PyTorch and customize CUDA implementations for sparse MHA and routed FFN because PyTorch does not support their underlying sparse operators. In particular, to identify the top- L attention weights for each token in MHA, we utilize the product quantization technique to quantize the tokens and measure the similarity between two tokens using their common codewords. This is efficient as it avoids computing and sorting floating point distances. By focusing on only the top- L attention weights, we can model the attention calculation as sparse matrix multiplications (e.g., SDDMM and SpMM) for efficiency. The routed FFN causes an efficiency challenge because different tokens activate different model parameters, and thus it is difficult to batch their computation. To tackle this problem, we design a novel blocked sparse matrix-vector multiplication (BSpMV) procedure, which batches the tokens that activate the same block in the model parameters for efficient computation.

We conduct extensive experiments to evaluate SPT and to compare with well-optimized full-parameter tuning and LoRA implementations. For end-to-end fine-tuning on two billion-parameter models, SPT achieves a maximum $1.47\times$ speedup with only marginal degradation to model quality. Considering five popular Transformer blocks with different configurations (e.g., embedding dimension and projection matrix size), SPT consistently outperforms full-parameter tuning and LoRA with $2.2\times$ speedup and uses 50% less memory, in the best cases. We also conduct micro experiments to validate our designs. The results show that the sparse MHA effectively reduces memory consumption, and the routed FFN effectively reduces running time. This can also be observed from Table 1, where SPT yields a larger performance gain over LoRA than LoRA over full-parameter tuning.

To summarize, we make the following contributions.

- We observe two key opportunities to improve LoRA fine-tuning, i.e., the memory consumption of MHA and running time of FFN.

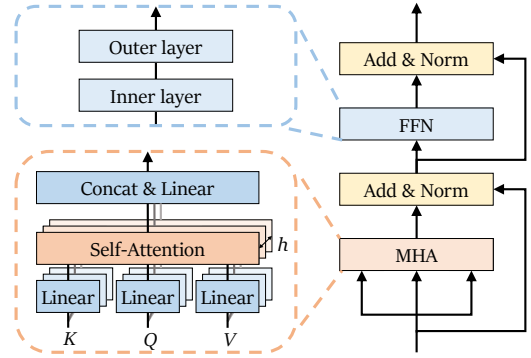


Figure 1: The structure of a Transformer block.

- By inducing sparsity, we propose the sparse MHA and routed FFN as two key modules to improve the efficiency of Transformer.
- To run our sparse modules efficiently, we adopt a suite of techniques such as product quantization, bucket-sort-based ranking, and block-based computation batching.
- We implement all these ideas in the SPT system on PyTorch and make it open-source¹ to benefit language model practitioners.

2 BACKGROUND

In this part, we introduce the basics of Transformer-based models and their fine-tuning to facilitate the subsequent discussions.

2.1 Transformer Basics

Transformer-based models (e.g., BERT [11], GPT [30], OPT [46], and LLaMA [40]) take a sequence of tokens (e.g., keywords in a paragraph) and produce an embedding vector for each token. This is achieved by passing the initial token embeddings through several Transformer blocks. As shown in Figure 1, each Transformer block has two main components, i.e., *multi-head attention* (MHA) and *feed-forward network* (FFN).

MHA involves multiple attention heads that work in parallel, and an attention head allows each token to aggregate all tokens in the sequence based on correlation (called ‘attend’ the tokens). In particular, the input of an attention head is $X \in \mathbb{R}^{n \times d}$, where n is the sequence length and d is the dimension of the embedding for each token divided by the total number of attention heads (called embedding dimension afterward). Each row $x_i \in \mathbb{R}^d$ of X corresponds to the input of a token to one attention head. The attention head uses learnable projection matrices W^Q , W^K , and W^V to project the input X to obtain query matrix Q , key matrix K , and value matrix V as follows

$$Q = XW^Q, \quad K = XW^K, \quad V = XW^V. \quad (1)$$

Then, the Q , K , and V matrices are used to compute output as

$$Y = \text{Attention}(Q, K, V) = \text{Softmax}(QK^T)V. \quad (2)$$

In particular, Eq. (2) uses Q and K to compute an attention weight matrix $A = \text{Softmax}(QK^T) \in \mathbb{R}^{n \times n}$, where an entry $a_{ij} \in A$ models the correlation between token i for token j . The final output is

¹GitHub repository: <https://github.com/ytgui/SPT-prot>

$Y = AV$, i.e., each row $y_i \in \mathbb{R}^d$ of the output matrix $Y \in \mathbb{R}^{n \times d}$ is a weighted sum of the rows in V . More specifically, y_i can be expressed as

$$y_i = \sum_{j=1}^n \frac{\exp(q_i^T k_j)}{\sum_{j=1}^n \exp(q_i^T k_j)} v_j, \quad (3)$$

where $a_{ij} = \exp(q_i^T k_j) / (\sum_{j=1}^n \exp(q_i^T k_j))$ is the attention weight of token i for token j produced by the softmax function and we can simplify Eq. (3) as $y_i = \sum_{j=1}^n a_{ij} v_j$.

The FFN stacks two linear mapping layers to map the embeddings, which are called inner projection and outer projection, respectively. That is,

$$H = \text{ReLU}(XW_I), \quad Y = HW_O, \quad (4)$$

where $W_I \in \mathbb{R}^{d \times D}$ and $W_O \in \mathbb{R}^{D \times d}$ are the parameters of the inner and outer projection matrices. The row dimension of W_I (i.e., d) matches the column dimension of X , and D is the intermediate dimension of FFN (usually larger than d). Note that MHA and FFN have different inputs and outputs although we use the same notations (i.e., X and Y) for conciseness.

2.2 Fine-tuning Transformer

Due to the high computation cost and massive size of general-purpose corpus, training Transformer-based models from scratch is prohibitively expensive. As a result, the standard practice when applying these models to a specific task is to fine-tune a pre-trained model. In particular, fine-tuning takes a pre-trained model and continues to train the model on a dataset collected for the target task (e.g., chatbot for makeup sales). Fine-tuning benefits from the substantial knowledge encoded in the parameters of the pre-trained model, while only required to train on a small task-specific dataset rather than a large general-purpose corpus.

During fine-tuning, one may directly update all the model parameters, which is called *full-tuning*. However, full-tuning is expensive because there are many model parameters to update. As such, adapter-based fine-tuning is proposed, which freezes the pre-trained model parameters and introduces a small number of new parameters that are updated to adapt to the target task [4]. The most popular adapter-based fine-tuning method is *low-rank adaptation* (LoRA) [18]. Consider a linear projection of the form $Y = XW$ (which serves as the basic unit for both MHA and FFN), where $X \in \mathbb{R}^{n \times d}$ is the input and $W \in \mathbb{R}^{d \times h}$ is the model parameter, LoRA describes the projection as

$$Y = XW + XBC = X(W + BC), \quad (5)$$

where W contains the pre-trained parameters and is kept fixed while B and C are the new parameters and are updated during training. Moreover, both $B \in \mathbb{R}^{d \times r}$ and $C \in \mathbb{R}^{r \times h}$ are low-rank matrices with $r \ll d$, and thus the number of parameters to update is small for efficient gradient computation and update. LoRA is shown to yield comparable model accuracy to full-tuning. Inference with LoRA model is as efficient as the original model because we can merge the pre-trained and new model parameters as $W' = W + BC$ after fine-tuning. Thus, we focus on improving LoRA fine-tuning in this paper.

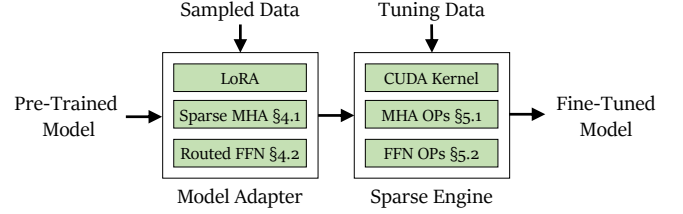


Figure 2: The workflow of our SPT system.

3 SPT SYSTEM OVERVIEW

Our SPT integrates algorithmic and systematic innovations to improve the efficiency of LoRA-based fine-tuning in terms of both running time and memory usage. Note that reducing memory usage, in addition to running time, is also critical when tuning Transformer models because peak memory scales with sequence length. By lowering memory demands, the same GPU can handle longer sequences with a fixed memory capacity; longer sequences provide more context for language models and enable more downstream tasks [2, 36]. As shown in §1, for LoRA fine-tuning, the main memory consumption comes from storing the attention matrix $A \in \mathbb{R}^{n \times n}$ for MHA while the main running time is consumed by FFN for the projections $Y = XW$. From the algorithmic perspective, we observe that *sparsification* effectively reduces both costs, i.e., memory consumption drops by keeping only some of the attention weights in A , and computation becomes faster by using only some of the parameters in W to conduct projection. Thus, we propose the sparse MHA and FFN modules to expose sparsity. From the system perspective, we build an efficient execution engine to run the sparse MHA and FFN modules on GPU, which is radically different from existing engines that use dense neural networks. Figure 2 provides an overview of SPT, and we briefly introduce its workflow as follows.

Model Adapter. It prepares a pre-trained Transformer-based model for sparse fine-tuning. First, the pre-trained model parameters are loaded, and then the LoRA layers and related new parameters are inserted into the computation graph of the model. It then replaces the standard MHA and FFN modules with our *sparse MHA* (cf. §4.1) and *routed FFN* (cf. §4.2).

In particular, sparse MHA replaces the dense attention computation $A = QK^T$ in Eq. (2) with sparse dense-dense matrix multiplication (SDDMM) $A' = \text{SDDMM}(Q, K^T)$, which computes only the top- L largest attention weights for each row q_i of the query matrix Q . As such, the sparse attention matrix A' has only $n \times L$ non-zero entries and takes much smaller space than the $n \times n$ dense attention matrix A . The output of sparse MHA is computed as $Y = A'V$ instead of $Y = AV$ in Eq. (2), and this is conducted by a sparse matrix-matrix multiplication (SpMM) $Y = \text{SpMM}(A', V)$. The routed FFN induces sparsity by using only some rows of the inner projection matrix W_I and columns of the outer projection matrix W_O . This reduces the computation workloads (i.e., XW_I and HW_O) in Eq. (4) for dense matrix multiplications. Note that instead of permanently removing some parameters for all tokens (which

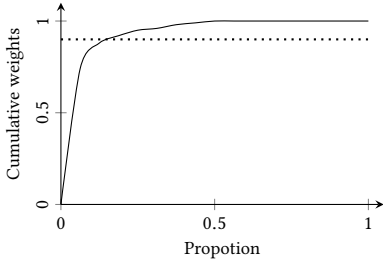


Figure 3: CDF of the softmax attention weights in MHA.

harms model quality), our routed FFN dynamically determines the parameters to prune for each token.

Sparse Engine. SPT implements an efficient computation engine to conduct fine-tuning on the modified computation graph. The engine is built on PyTorch [29] and includes customized CUDA implementations for the sparse operators, which are not supported by PyTorch. For sparse MHA, the key challenges are finding the top- L keys for each query and conducting SDDMM and SpMM for sparse attention efficiently. We adapt the product quantization method to map the queries and keys and propose a bucket-sort-based procedure for top- L selection; we also carefully design the index encoding for the sparse matrices to make SDDMM and SpMM efficient (cf. §5.1). For routed FFN, the key challenge is that different tokens activate different model parameters, which invalidates efficient batched computation. We design a novel blocked sparse matrix-vector multiplication (BSpMV) procedure, which batches the tokens that activate the same block in the model parameters for efficient computation (cf. §5.2).

SPT allows users to trade-off between training efficiency and model quality by configuring the strength of sparsification. This is done by setting L (i.e., the number of attention weights to consider for each query vector in MHA) and β (i.e., the portion of model parameters to use for FFN). As we will show by experiments in §6, SPT can significantly improve efficiency with only a marginal degradation to model quality. To help users determine the strength of sparsification, SPT allows users to conduct short training trials on some sample data.

4 THE SPARSE TRANSFORMER

In this part, we introduce our two key sparse modules for Transformers, i.e., sparse multi-head attention (MHA) and routed feed-forward network (FFN).

4.1 Sparse Multi-head Attention

Sparse attention. We observe that the output of an attention head can be approximated by considering only the top- L attention weights for each query vector q_i . Recall that the i^{th} output embedding (i.e., the i^{th} row of the output matrix Y) of MHA can be expressed as

$$y_i = \sum_{j=1}^n a_{ij} v_j,$$

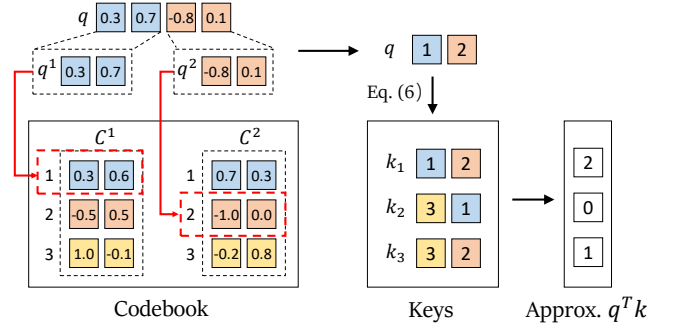


Figure 4: An illustration of PQ.

where attention weight $a_{ij} = \exp(q_i^T k_j) / (\sum_{j=1}^n \exp(q_i^T k_j))$ is computed using the softmax function, which normalizes the scores $\exp(q_i^T k_j)$ across all keys k_j for each query q_i . This gives a probability distribution over the keys for each query as softmax ensures that the attention weights for each query sum to 1. The relative weight $a_{ij'}/a_{ij} = \exp(q_i^T k_{j'} - q_i^T k_j)$ depends only on the relative scores $q_i^T k_{j'} - q_i^T k_j$ for two keys j' and j . If $q_i^T k_{j'}$ is moderately larger than $q_i^T k_j$, $a_{ij'}/a_{ij}$ will be large as function $\exp(x)$ increases quickly with x . Thus, for each query q_i , the keys with the highest dot product score $q_i^T k_j$ will dominate the attention weights.

Figure 3 shows this phenomenon by plotting the cumulative distribution function (CDF) of the attention weights, where the top-15% attention weights take up 90% of the total attention weights. As attention weights beside the top- L are small, we can approximate y_i as $y_i' = \sum_{j \in S_k} a_{ij} v_j$, where S_k denotes the set of keys with the top- L scores for q_i . We also revise softmax as $a_{ij} = \exp(q_i^T k_j) / (\sum_{j \in S_k} \exp(q_i^T k_j))$ such that the attention weights of the top- L keys sum to 1. This approximation makes the attention matrix sparse to save memory consumption as most attention weights are treated as 0.

PQ for efficient sparsification. Identifying the top- L attention scores for q_i is essentially the maximum inner product search (MIPS) problem, which, given a query vector q , finds the top- L vectors having the maximum inner product with q in a dataset containing n vectors [34, 39]. A naive solution will first compute the scores for all keys and then identify the top- L . This introduces high computation costs. Pre-indexing k_j , as vector databases do for efficient top- L retrieval, with techniques such as proximity graphs and trees, is also not feasible, because the keys are generated dynamically by MHA. Fortunately, there are many approximate solutions to MIPS, which find the most (rather than all) of the top- L to trade for efficiency [20]. We utilize the *product quantization* (PQ) technique as our approach because it is computationally lightweight and can run efficiently on GPU.

PQ quantizes a vector $q \in \mathbb{R}^d$ using M codebooks C^1, C^2, \dots, C^M . Each codebook C^m contains E codewords and each codeword is a $d' = d/M$ -dimensional vector, i.e., $C^m = \{c^m[1], c^m[2], \dots, c^m[E]\}$ with $c^m[e] \in \mathbb{R}^{d'}$ for $1 \leq m \leq M$ and $1 \leq e \leq E$.² Vector q is first chopped into M sub-vectors $[q^1, q^2, \dots, q^M]$ with each sub-vector

²We assume that d is divisible by M . If this does not hold, PQ usually allocates fewer dimensions to the last codebook. This subtlety does not affect our discussions.

Algorithm 1 The procedure of sparse MHA.**Input:** the query, key, and value embeddings Q, K, V **Output:** attention output Y

- 1: Quantize the query vectors $C_Q \leftarrow \text{quantize}(Q)$
- 2: Quantize the key vectors $C_K \leftarrow \text{quantize}(K)$
- 3: Select the top- L keys for each query $\tilde{Q}, \tilde{K} = \text{select}(C_Q, C_K)$
- 4: Compute sparse attention weight $\tilde{A} \leftarrow \text{softmax}(\tilde{Q}\tilde{K}^T)$
- 5: Compute attention output $Y \leftarrow \tilde{A}V$

$q^m \in \mathbb{R}^{d'}$. Then, each sub-vector q^m of q is approximated by finding the codeword with the minimum Euclidean distance to it in codebook C^m . Denote t_q^m as the index of such codeword in codebook C^m , q is approximated by concatenating the codewords from each codebook $\tilde{q} = [c^1[t_q^1], c^2[t_q^2], \dots, c^M[t_q^M]]$. Figure 4 provides a running example of PQ with 2 codebooks and each codebook containing 3 codewords. In particular, q finds codeword $t_q^1 = 1$ in codebook C^1 and codeword $t_q^2 = 2$ in codebook C^2 , and thus $\tilde{q} = [c^1[1], c^2[2]] = [0.3, 0.6, -1.0, 0.0]$.

With PQ, the query-key inner product $q^T k$ can be approximated as $\tilde{q}^T \tilde{k}$ using the quantized representations of the query and key. This approximation is typically computed by looking up an inner product table for each codebook and summing up the terms from all codebooks as $\tilde{q}^T \tilde{k} = \sum_{m=1}^M c^m[t_q^m]^T c^m[t_k^m]$, where $c^m[t_q^m]^T c^m[t_k^m]$ is pre-computed for all codeword combinations. However, performing both this summation and the subsequent top- L identification with floating point numbers is expensive. We propose conducting similarity computation with integers for improved efficiency. Specifically, given that $\tilde{q} = [c^1[t_q^1], c^2[t_q^2], \dots, c^M[t_q^M]]$ and $\tilde{k} = [c^1[t_k^1], c^2[t_k^2], \dots, c^M[t_k^M]]$, we approximate $q^T k$ as

$$s(q, k) = \sum_{m=1}^M \mathbb{I}[t_q^m = t_k^m], \quad (6)$$

where $\mathbb{I}[\cdot]$ is the indicator function. The intuition is that if q and k are mapped to the same codeword in more codebooks, they are more likely to have a large inner product. A running example is provided in the right part of Figure 4, where the codeword indexes of q are compared to 3 keys. As both computing and ranking the scores involve only integers, we adopt an efficient bucket-sort-based algorithm in §5 for top- L selection. This approximation also provides good accuracy and the recall rate of identifying top- L is close to 90%, which is essential for good model quality.

Workflow. Algorithm 1 summarizes the procedure of our sparse MHA. First, the query and key vectors are quantized by the PQ codebooks (line 1 and 2). Second, we identify the top- L query-key pairs according to the PQ codewords using Eq. (6) (line 3). Then, we compute the sparse attention matrix according to the top- L query-key pairs (line 4) and the final output (line 5). Here line 4 and line 5 involve sparse matrices instead of dense matrices as in the original MHA, and thus we develop specialized implementations in §5. Note that Transformers can be categorized into Encoders or Decoders, distinguished by whether there is a look ahead mask to prevent attending to future tokens. SPT can be utilized in both the

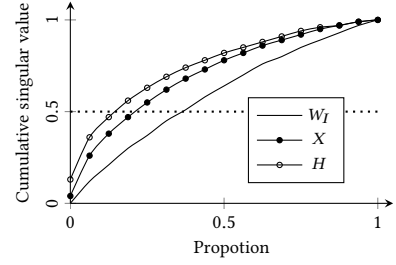


Figure 5: CDF of the normalized singular values in FFN.

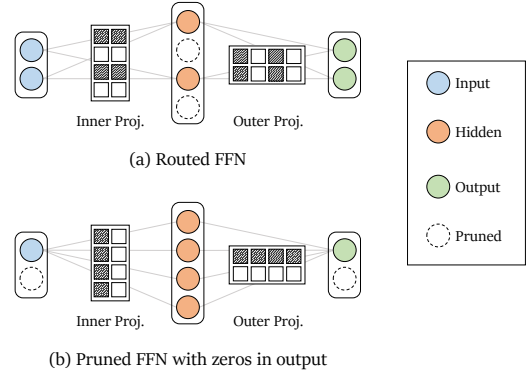


Figure 6: An illustration of the routed FFN.

Encoder and Decoder architectures, we achieve this by applying the look ahead mask when computing softmax.

Complexity analysis. Assuming that the sequence length is n and the embedding dimension is d for a single head, the original attention has time complexity $O(n^2 d)$ to compute all scores and space complexity $O(n^2)$ to store the attention weights. For PQ with M codebooks each containing E codewords, the time to quantize the keys and queries is $O(ndE)$; the time to select the top- L keys for all queries is $O(n^2)$; and finally computing the top- L attentions take time $O(nLd)$; thus the overall time complexity is $O(ndE + n^2 + nLd)$. The space complexity is $O(nL)$ to store the attention weights and $O(Ed)$ to store the codebooks. We set the number of codewords E as a small number (e.g., 16 and 32, which allows ignoring the terms involving E), the value of L in top- L as λn . Thus, the space complexity of sparse MHA is roughly $O(\lambda n^2)$. For instance, $\lambda = 0.25$ yields a memory saving of 75%.

4.2 Routed Feed-forward Network

To reduce the computation cost of FFN, we prune a portion of its parameters, which means that only a subset of the parameters are activated for computation. Weight pruning techniques are widely used to improve efficiency for neural network models [42], and they fall into two main categories, i.e., static pruning and dynamic pruning. Static pruning removes weights from the model based on their importance (e.g., magnitude) and does not consider the input. Dynamic pruning makes the pruning input-aware by removing different weights for different inputs.

We conducted an empirical study to determine whether FFN should use static pruning or dynamic pruning. Figure 5 plots the CDF of the singular values of the inner projection matrix, feature matrices before and after the projection (the *ReLU* activation is not considered). Specifically, we use the FFN in the last Transformer block of the OPT-2.7B model and set the sequence length as 512 without padding. Figure 5 shows that the inner projection matrix (i.e., W_I) has a high-rank, and the cumulative singular value increases almost linearly with the number of singular values. This indicates that the projection matrix utilizes most of its model capacity (i.e., small redundancy). However, the projection output (i.e., H) has a relatively low-rank, with the top 25% singular values taking up more than 50% of the energy. Similar observations are also made on other FFN blocks and different Transformer architectures. These results suggest that static pruning on weight matrices will harm model capacity and degrade quality, while the projection output has a low-rank and can be pruned by inducing sparsity. As such, we select the dynamic pruning strategy, which keeps the capacity of W_I and derives sparsity on H .

Dynamic routing. The question becomes how to conduct dynamic pruning while still supporting efficient computation. The naive solution is to prune the individual entries in the projection matrices. However, this induces highly irregular sparsity (as in our sparse MHA) and makes it inefficient to run the sparsified model. As such, we use a block-based pruning strategy, which organizes adjacent rows and columns of the projection matrices as a block and conducts pruning at block granularity. This means that entries inside a block are activated together and can be handled by dense matrix computation effectively on GPU.

In particular, for an FFN whose inner projection is $h = \text{ReLU}(xW_I)$ and outer projection is $y = \text{ReLU}(xW_O)$, we prune the rows of the inner projection matrix and the columns of the outer projection matrix as shown in Figure 6a. As can be observed from Figure 6a, pruning the row of W_I sets some entries of the indeterminate embedding h to zero, which means that the corresponding columns of W_O will not be used to compute the final output embedding y . The converse strategy shown in Figure 6b, i.e., pruning the columns of W_I and rows of W_O , does not work because it means that some of the input dimensions are not used to compute the intermediate output h and some dimensions of the final output y are zero. This severely reduces model capacity and thus degrades model quality.

The final problem becomes how to choose the blocks to prune. We cannot compute the exact output y and then select the smallest output dimensions because this does not save computation. Thus, we train a small *route network* to guide pruning. Specifically, assuming that W_I has D rows, we organize the rows into G groups by assigning D/G adjacent rows to each group. The route network is a single layer feed-forward network $x_R = xW_R$ with $W_R \in \mathbb{R}^{d \times G}$, where d is the embedding dimension; and we set the top G' entries in x_R with the largest magnitude (and the corresponding row groups in W_I) as activated. Note that the activated groups of W_O are decided according to the activated groups of W_I , and thus we do not need another route network for W_O . We use a small G (e.g., 4 or 8) such that the route network is cheap to compute. The route network is trained along with the FFN such that it can learn to determine the weight groups to activate. We introduce a load-balancing loss

Algorithm 2 The procedure of PQ quantization.

Input: the vectors to quantize X , and the codebooks C

Output: the codewords C_X and quantization errors e_X for X

```

1: for subspace from  $i = 1$  to  $M$  do
2:   Compute distances  $Dist_i \leftarrow \text{cdist}(X_i, C_i)$ 
3:   Get centroids  $C_X[i] \leftarrow \text{argmin}(Dist_i, \text{dim} = -1)$ 
4:   Select codewords  $Codex[i] \leftarrow \text{index\_select}(C_i, C_X[i])$ 
5:   Compute errors  $e_X \leftarrow \text{DKM}(Codex[i], X_i)$ 
6: end for
```

for the route network to ensure that the weight groups have similar activation rates and that the model capacity is fully utilized.

5 SPARSE EXECUTION ENGINE

To implement SPT, we utilize PyTorch’s existing modules such as embedding layers, fully connected layers, and back-propagation training. However, PyTorch does not support the sparse MHA and routed FFN modules we proposed in Section 4. Thus, we customize CUDA implementations for the two modules and discuss the key optimizations in this part.

5.1 Sparse MHA

Recall that our sparse MHA takes 3 steps, i.e., quantizing the query and key vectors using PQ codebooks, finding the top- L query-key pairs based on PQ quantization, and finally computing sparse attention for the top- L query-key pairs. We customize the 3 steps on GPU to make sparse MHA efficient.

PQ quantization. We use Algorithm 2 to quantize the query and key vectors, and each vector is mapped to its nearest codewords in the M codebooks. The vectors of a sequence are processed together for one codebook at a time, and thus the input dimension of the distance computation operator (*cdist*) is [sequence length, dim codeword], which contains a subspace of all the input vectors; the dimension of a codebook is [num codewords, dim codeword], and the distance output is of size [sequence length, num codewords]. The *argmin* operator finds the nearest codeword for each input vector in the codebook, and the output dimension is [sequence length, 1]. We utilize the differentiable k-means (DKM) [6] algorithm to adjust the codebook, which allows the codebook to match data distribution and requires the computation of the quantization error (i.e., the distance between a vector and its nearest codeword).

We set the codeword dimension of each codebook (i.e., d') to 8 and codebook size (i.e., the number of codewords in each codebook) to 16. Using more codewords improves quantization accuracy but also increases computation cost. We observe that 16 codewords already yield good model quality as the softmax output of attention tends to converge to a small number of high probability values. We accelerate Algorithm 2 with two implementation optimizations. First, we perform codebook update every 20 mini-batches instead of every mini-batch, which means that Lines 4-5 of Algorithm 2 are skipped to reduce computation for most mini-batches. This does not harm model quality because the codebooks represent centroids of the query and key vectors, which change slowly over mini-batches. Second, the *cdist* and *argmin* operators are fused into one CUDA kernel. This avoids producing the intermediate results for *cdist*,

Algorithm 3 The procedure of top- L selection.**Input:** the codewords C_Q, C_K for the query and key vectors**Output:** the position of top- L query-key pairs as $Indices$

```

1: for all query codeword  $c_q$  in  $C_Q$  do
2:    $Ptr \leftarrow \text{allocate}(M + 1), Bucket \leftarrow \text{allocate}((M + 1) \times L)$ 
3:   for all key codeword  $c_k$  in  $C_K$  do
4:      $s \leftarrow \text{indicator}(c_q, c_k)$   $\triangleright$  Distance with PQ code
5:      $ptr \leftarrow Ptr[s]$   $\triangleright$  Position to store the key
6:      $Bucket[s][ptr] \leftarrow$  the index of key
7:      $Ptr[s] \leftarrow \min(ptr + 1, L - 1)$   $\triangleright$  Prevent overflow
8:   end for
9:    $s \leftarrow M, ptr \leftarrow 0$   $\triangleright$  Pointer used to read from  $Bucket$ 
10:  for all  $i = 0$  to  $L - 1$  do
11:    if  $ptr$  equals  $Ptr[s]$  then  $\triangleright ptr$  reaches the end
12:       $ptr \leftarrow 0, s \leftarrow s - 1$   $\triangleright$  Move to the previous bucket
13:    end if
14:     $Indices_q[i] \leftarrow Bucket[s][ptr + +]$   $\triangleright$  Write result for  $q$ 
15:  end for
16: end for

```

whose size is large (i.e., [sequence length, num codewords]), and thus reduces memory access.

Top- L selection. For the query and key vectors of a sequence, we use Algorithm 3 to find the top- L most similar key vectors for each query vector. The procedure works as follows.

- *Initialize (line 2).* As each query and key vector is quantized to M codewords, we use the number of common codewords (i.e., indicator in line 4) to measure their similarity. Since the possible values of common codewords fall in $\{0, M\}$, we allocate $M + 1$ empty buckets, indexed from $Bucket[0]$ to $Bucket[M]$, to hold the keys with the corresponding similarity scores for each query vector. We set the capacity of each bucket as L such that each bucket can hold all the top- L keys in the worst case.
- *Assign (lines 3-8).* The algorithm goes over the keys to compute the similarity scores. For a key with score s , it is put into $Bucket[s]$ (line 6); and we use $Ptr[s]$ to record the next position to insert for $Bucket[s]$. If a bucket already contains L keys, we overwrite an old key with the new key to avoid bucket overflow (line 7). This is because only L top keys are required and dynamically allocating memory on GPU is impossible. At this time, the algorithm groups keys together, enabling top- L selection from the buckets.
- *Retrieve (lines 9-16).* We retrieve the top- L similar keys for each query vector by checking the buckets from high index to low index (i.e., $Bucket[M]$ to $Bucket[0]$). This is because the keys in higher buckets have larger similarity scores w.r.t. the query vector. This process stops when L keys are collected. Note that we do not need to perform a full sort within each bucket as in classical bucket sort.

Algorithm 3 is efficient for GPU execution. The outer loop (line 1) can be easily parallelized by GPU threads, i.e., each query vector is processed by one GPU thread in parallel. We also parallelize the inner loops (lines 3 and 10) by scheduling two extra GPU threads to process different bucket elements, i.e., one thread handles odd

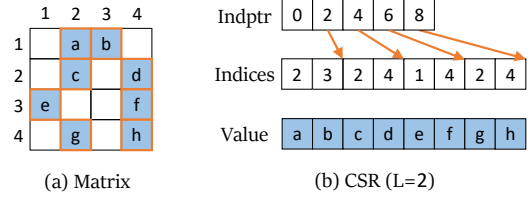


Figure 7: CSR encoding from the top- L query-key pairs, the non-zero entries are colored.

indices and the other handles even indices. Moreover, we allocate the buckets in fast on-chip shared memory and only move the final top- L query-key pairs to global memory when collecting the results. This requires only one sequential write and has a small memory access overhead. Last but not least, our bucket-sort-based top- L selection is much more efficient than using the standard approximate distance of PQ, which computes and sorts floating point distances.

Sparse attention computation. We utilize sparse operations to compute the sparse attention matrix and the attention outputs. In particular, sampled dense-dense matrix multiplication (SDDMM) is used to compute the attention weights between the top- L query and key pairs. Sparse matrix-matrix multiplication (SpMM) is used to multiply the sparse attention weights with the value vectors to generate the attention outputs. Instead of implementing SDDMM and SpMM from scratch, we adapt NVIDIA’s cuSPARSE library.

The cuSPARSE library allows storing sparse matrices using either the compressed sparse row (CSR) format or coordinate list (COO) format, which has different performance characteristics. In particular, CSR stores row pointers ($Indptr$) and column indices ($Indices$), and thus is efficient for row-major arithmetic operations like matrix multiplication. COO stores the row and column coordinates and makes it simple to construct a sparse matrix. We choose the CSR format for the sparse matrices because it is efficient for row-oriented attention computation.

The CSR matrix used for SDDMM and SpMM is constructed directly from the output of the previous top- L selection step. As shown in Figure 7, the $Indices$ array of CSR stores the column indices of the non-zero values (i.e., top- L keys), which is the output of the top- L selection step. The $Indptr$ array marks the start and end positions of the $Indices$ for each row. Since we select L keys for each query vector, the $Indptr$ array is $[0, L, 2L, 3L, \dots]$. Note that we only need to construct the CSR matrix once and reuse it for both SDDMM and SpMM, this is because the sparse matrix produced by SDDMM (i.e., the attention matrix) serves as the input to SpMM (i.e., for final attention output), and the *softmax* function does not change the matrix shape.

5.2 Blocked Sparse Matrix-Vector Multiply

The standard dense FFN layer takes the token sequences as input and performs batched matrix multiplications between the input tokens and the weight matrices. Our routed FFN layer activates different subsets of the weight matrices for each input token, i.e., different tokens interact with different weight matrices. This leads

Algorithm 4 The procedure of BSpMV.

Input: token sequence X , model weight matrices W_I , W_O , and $Indices$ of the activated model weight blocks for the tokens

Output: a new sequence representation Y

- 1: **for** block from $i = 1$ **to** G **do**
- 2: Generate token mask $Mask_T \leftarrow \text{eq}(Indices, i)$
- 3: Select tokens $X_i \leftarrow X[Mask_T]$
- 4: Compute inner projection $H \leftarrow \text{ReLU}(X_i W_I[i])$
- 5: Compute outer projection $Y[Mask_T] \leftarrow H W_O[i]$
- 6: **end for**

to a general sparse-dense matrix-vector multiplication problem that invalidates batched matrix multiplications and harms efficiency.

A naive solution is to generate a binary mask matrix that indicates the activated weights for each input token, and these masks are multiplied with the weight matrices in an element-wise manner before batch computation. This solution has high memory consumption because it stores a separate mask for each input token. To reduce memory consumption, one may use the block-compressed sparse row (BSR) matrix format to store the masks. Like CSR, BSR stores only the nonzero entries but each entry corresponds to a sub-matrix instead of scalar values. For a sequence length n and number of blocks \hat{B} , BSR requires $O(n\hat{B})$ space. BSR is still inefficient because duplicating the weight matrices for each token has a high overhead.

We propose an efficient blocked sparse matrix-vector multiplication (BSpMV) method to perform batched multiplications between sparse FFN matrices and vectors. The insight is that the sparsity induced by our routed FFN actually means that each dense block of weights is only relevant for computing the outputs for a subset of the input tokens. In particular, as shown in Algorithm 4, we iterate over the weight blocks (line 1) and select a subset of token vectors (line 3) to perform dense matrix computation with the block (lines 4 and 5). Our BSpMV approach has several benefits: (1) it can leverage fast dense GEMM computations for each block; (2) the processing of different weight blocks can be parallelized across GPU streams; (3) the number of blocks is small, and thus it is fast to loop over them; (4) each block in the iteration can compute some output results without synchronizing with the other blocks. BSpMV needs to extract the relevant token vectors for each block but the overhead is small.

6 EXPERIMENTAL EVALUATION

In this part, we evaluate the efficiency and effectiveness of SPT with extensive experiments. The key findings are that:

- SPT outperforms both full-parameter tuning and LoRA fine-tuning across all model configurations, with a maximum running time speedup of 2.2 \times and peak memory reduction of 50%.
- Our two key optimizations (i.e., sparse MHA and routed FFN) and their implementations are effective in improving efficiency.

6.1 Experiment Settings

Models. We use two well-known Transformer-based large language models to evaluate the performance of end-to-end fine-tuning, i.e.,

Table 2: Statistics of the Transformer blocks in experiments.

Name	d_{model}	d_{head}	d_{ffn}	Pre-trained Model
OPT-1024	1024	64	4096	GPT2-medium, OPT-350M
OPT-2048	2048	64	8192	OPT-1.3B
OPT-2560	2560	80	10240	OPT-2.7B
LLaMA-2560	2560	128	6912	Sheared-LLaMA-2.7B
LLaMA-4096	4096	128	11008	Open-LLaMA-7B

OPT-2.7B [46] and LLaMA-2.7B [43]. In particular, OPT-2.7B stacks 32 Transformer blocks, and uses the ReLU activation function and a simple feed-forward structure. LLaMA-2.7B also stacks 32 Transformer blocks but uses the GeLU activation function and rotary positional embeddings [35]. We also experiment with the 5 Transformer configurations in Table 2 to evaluate the performance of individual Transformer blocks. In particular, d_{model} is the embedding dimension size of the Transformer models (including multi-heads), d_{head} represents the token embedding size of a single attention head, which corresponds to d in §2.1, and d_{ffn} means the hidden dimension size in FFN. These Transformer blocks come from popular language models listed in the last column of Table 2 and thus are representative of Transformer configurations.

Datasets. We use the following 3 datasets for the experiments.

- *Massive Multi-task Language Understanding* (MMLU) [16] is a popular dataset for question answering, where 4 choices are provided for each question and the model is trained to select an answer for each question. It uses a metric also called MMLU to evaluate the question answering accuracy of the models, and a higher MMLU refers to better model quality.
- *Wikitext-103* [27] is a widely used dataset for next-word prediction training. Collected from Wikipedia, it contains over 100 million tokens. Wikitext-103 is an unlabeled dataset and thus we use perplexity (PPL) as an evaluation metric to assess the model quality. A smaller PPL score indicates that the language model fits the training data better and has lower losses.
- *Random* contains randomly generated sequences of arbitrary length that can be specified as needed. We mainly use it for micro experiments due to this flexibility.

Baselines and platform. We compare the SPT system with full-parameter tuning (i.e., *Full*) and LoRA fine-tuning (i.e., *LoRA*), both of which have been well implemented and extensively optimized. By default, the sparse MHA of SPT uses the top-1/8 attention weights for each query and the routed FFN activates 1/2 of the parameters in the projection matrices. Our experiment platform is a server with 4 NVIDIA RTX3090 GPUs (each with 24GB global memory), dual Intel Xeon Gold 6326 CPU, and 256 GB main memory. All the experiments are conducted with single-precision floating point numbers, and weight decay is enabled for the optimizer.

6.2 Main Results

End-to-end fine-tuning. In this experiment, we conduct end-to-end fine-tuning for the OPT-2.7B and LLaMA-2.7B models on the MMLU dataset. To emulate real-world fine-tuning scenarios, we

Table 3: End-to-end fine-tuning results. MMLU indicates model quality, and the speedups are over Full.

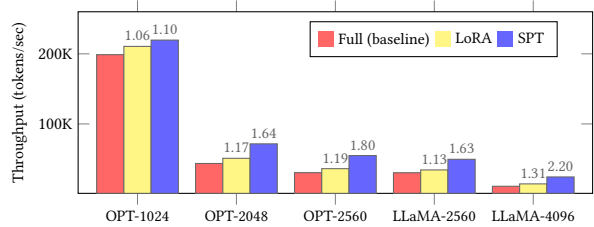
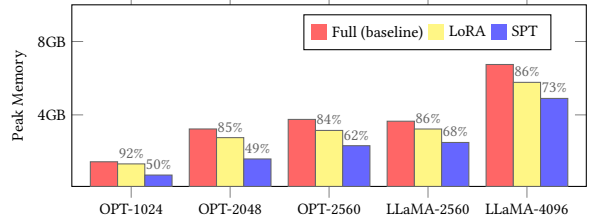
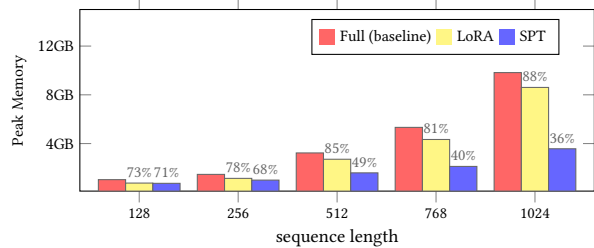
Model	System	MMLU	Max Length	Time (speedup)
OPT-2.7B	Full	27.0	256	6.7 h (1.00x)
	LoRA	27.0	512	5.8 h (1.15x)
	SPT	26.1	768	4.6 h (1.47x)
LLaMA-2.7B	Full	29.0	256	6.9 h (1.00x)
	LoRA	29.0	384	5.8 h (1.18x)
	SPT	28.4	640	5.0 h (1.39x)

employ all 4 GPUs on our system and use DeepSpeed [31] for multi-GPU capabilities. Note that DeepSpeed has a sophisticated memory management mechanism for multi-GPU configuration, and we enable parameter and activation offloading in DeepSpeed from GPU memory to CPU memory to reduce GPU memory footprint. As a result, we are unable to measure the peak memory consumption on GPUs. To understand the memory constraints of the baselines, we utilize the maximum sequence length (Max Length) without triggering an out-of-memory (OOM) error as a surrogate. DeepSpeed produces an OOM error when a single Transformer block cannot fit into GPU memory. We adjust the sequence length in increments of 128 until this OOM state occurs. Note that to ensure a fair comparison, we run all baselines with a sequence length of 512 and measure the 5-shot learning capabilities of MMLU. Each model is trained for 10k mini-batches with a batch size of 16.

The results in Table 3 show that SPT reduces running time and increases maximum sequence length compared with both full-parameter tuning and LoRA. Regarding running time for the two models, SPT speeds up full-parameter tuning by 1.47x and 1.39x. SPT is also 1.28x and 1.18x faster than LoRA. This is remarkable because the speedup of SPT over LoRA is larger than LoRA over full-parameter tuning. Moreover, SPT supports 2x sequence length compared with full-parameter tuning and over 1.5x compared with LoRA, which indicates a significant memory saving. Considering model quality, a small model quality degradation is observed in SPT in terms of MMLU decrease. Thus, SPT achieves a good trade-off between efficiency and model quality.

Transformer blocks. To understand the performance gains over individual Transformer blocks, we evaluate SPT on the 5 different Transformer configurations listed in Table 2. We use randomly generated sequences to easily control the experiment settings and run the evaluations on a single GPU to eliminate the overhead of multi-GPU communication. We transform the running time, i.e., time to compute the forward and backward passes for a Transformer block, into throughput (i.e., tokens processed per second) for more intuitive comprehension of the speedups. All results are averaged over 20 runs.

As reported in Figure 8, SPT yields consistent benefits in terms of throughput speedup (i.e., shorter training time) and lower peak memory requirements than full-parameter tuning and LoRA for all the configurations. Specifically, SPT achieves higher throughput than full-parameter tuning, with speedups ranging from 1.10x to 2.20x. It also outperforms LoRA, with throughput improvements

**(a) Training throughput for different Transformer blocks, the speedups are over full-parameter tuning.****(b) Peak memory consumption for training the 5 Transformer blocks, the percentages are over full-parameter tuning.****Figure 8: Fine-tuning throughput and peak memory for 5 Transformer blocks (batch size 16, sequence length 512).****Figure 9: Peak memory requirements when using different sequence lengths (OPT-2048, batch size 16).**

of 1.04x to 1.68x. The maximum speedup is observed on LLaMA-4096. This is because LLaMA-4096 has the largest FFN dimension (cf. Table 2) among the given Transformer settings, where FFN becomes dominant and exposes more optimization opportunities for the routed FFN module. On the other hand, SPT has much lower peak memory usage than the other systems. Specifically, it uses only 50% to 73% peak memory compared with full-parameter tuning, and 54% to 85% with LoRA. The largest peak memory reduction is observed on OPT-1024. This is because OPT-1024 has the smallest FFN dimension while MHA dominates most of the peak memory requirements, and thus the memory saving of our sparse MHA is significant. We also observed that varying both the sequence length and batch size did not impact the speedup provided by the SPT. This is mainly due to the routed FFN treating all additional dimensions as batches of tokens. The speedup stays consistent regardless of sequence length or batch size changes. Note that the speedups of SPT shown in Figure 8 are generally higher than those in Table 3. This is because factors like cross-GPU communication slowdowns

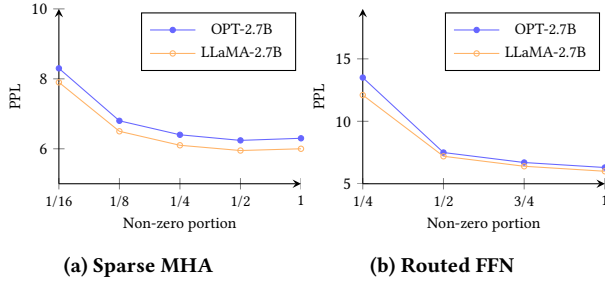


Figure 10: The influence of sparsity on model quality.

the end-to-end tuning, where these costs are not reduced by our optimizations.

Figure 9 shows that the peak memory consumption rises rapidly as the sequence length grows. This is because the attention matrix grows quadratically with sequence length. LoRA reduces memory consumption compared with full-parameter tuning, but the effect is limited. In comparison, SPT achieves more substantial memory savings for longer sequences as a result of MHA becoming more predominant. We also varied the batch size and found that it had minimal impact on the memory performance, since the MHA operates along the sequence dimension. Increasing the batch size does not affect the mechanism itself.

Discussions. LoRA states to reduce hardware requirements (especially memory) by using much smaller trainable parameters [18]. However, the memory savings of LoRA are not obvious in our experiments, e.g., taking up 84% to 92% of full-parameters tuning in Figure 8, this is because we use a relatively large batch size, and intermediate activations (rather than model parameters) dominate memory consumption in the case. For example, consider a fully connected (FC) layer with dimension 4096×1024 , the model parameters take $4M$, which can be saved by LoRA. However, with a batch size of 16 and sequence length of 512, the activations take up $16 \times 512 \times 4096 = 32M$, which are much larger than the parameters and can not be saved by LoRA. In contrast, the sparse MHA of SPT reduces the attention weights for each sequence, and thus consistent memory reduction is achieved at any batch size. Moreover, SPT has limited speedups when fine-tuning under extreme conditions, e.g., a batch size of 1, sequence length of 64, and FFN hidden dimension of 128. This is because when the total number of tokens input to the model is small, the optimization opportunities for routed FFN are limited. However, these cases are rare in practice, and the trends are to use longer sequences to capture richer contexts and larger FFNs to increase model capacity. Thus, SPT may yield even more significant efficiency gains for larger models that will come in the future.

6.3 Parameter Sensitivity and Design Choices

Model quality. In this experiment, We test the quality impact of SPT under different sparsity strengths. In particular, the sparsity of MHA is specified by the portion of non-zero attention weights, while the sparsity of routed FFN is determined by the portion of activated model parameters. We run this experiment using the Wikitext-103 dataset and evaluate PPL to measure model quality.

Table 4: The running time and peak memory consumption of MHA and FFN when using different sparsity.

(a) OPT-2048			
Module	Method	Peak Mem	Duration
MHA	LoRA	2626 MB	52.5 ms
	LoRA (compiled)	2418 MB	47.1 ms
	SPT (1/4)	1784 MB	72.9 ms
	SPT (1/8)	1123 MB	54.1 ms
FFN	LoRA	1106 MB	108.5 ms
	LoRA (compiled)	1106 MB	107.9 ms
	SPT (3/4)	993 MB	84.6 ms
	SPT (1/2)	928 MB	54.9 ms
(b) LLaMA-4096			
Module	Method	Peak Mem	Duration
MHA	LoRA	3799 MB	205.2 ms
	LoRA (compiled)	3478 MB	179.8 ms
	SPT (1/4)	3253 MB	238.4 ms
	SPT (1/8)	2711 MB	185.2 ms
FFN	LoRA	3329 MB	300.1 ms
	LoRA (compiled)	3502 MB	296.6 ms
	SPT (3/4)	2972 MB	228.9 ms
	SPT (1/2)	2811 MB	150.8 ms

Note that PPL is a strict measurement as it exponentiates the loss. Therefore, small differences in loss can result in large differences in PPL. The increasing PPLs shown in Figure 10 stabilize when the non-zero portion reaches 1/8 for sparse MHA and 1/2 for routed FFN. This indicates that our default sparsity strengths achieve a good balance between quality and efficiency. Here MHA allows higher sparsity than FFN because (1) there are multiple attention heads, which can complement each other to combat the information loss caused by sparsifying, and (2) the attention weights produced by the softmax function are more skewed than the FFN projection as we have shown in § 4, thus using sparse MHA yields less information loss.

Time and memory costs. In this experiment, we look into the time and memory consumption of MHA and FFN to validate the effectiveness of our optimizations. We adopt the same batch size and sequence length settings as in 6.2 and report the results in Table 4. Entries marked with *compiled* means that they are compiled with JIT, an option provided by the latest PyTorch. For SPT, the numbers in the brackets are the sparsity strengths used for MHA and FFN, and we set them as practical values that yield good model quality. We make the following observations from Table 4.

First, the sparse MHA effectively reduces the peak memory consumption compared with LoRA, and the reduction is larger with stronger sparsity. Specifically, considering OPT-2048, the reduction is 32% with a non-zero portion of 1/4 and 57% with 1/8 non-zeros. This, as explained in Section 4, sparse MHA only stores the top attention weights while standard MHA stores the attention weights between all token pairs, and stronger sparsity means that fewer attention weights are stored. Note that the sparse MHA has lower

Table 5: Breaking the computation time down to kernels for MHA and FFN.

Method	Part	Description	Kernel	Duration	Ratio
LoRA	MHA	LoRA matrix decomposition and multi-head feature transformation	sgemm_128x64_tn	13.5 ms	64.6%
		Multi-head attention calculation	sgemm_128x128_nn	2.8 ms	13.1%
			softmax_warp_forward	0.9 ms	4.2%
	Reshape, addition, or activation operators		elementwise_kernel	1.3 ms	6.0%
	FFN	LoRA matrix decomposition and feedforward feature transformation	sgemm_128x64_tn	13.8 ms	47.6%
			sgemm_128x128_tn	13.8 ms	47.6%
Reshape, addition, or activation operators		elementwise_kernel	1.1 ms	3.9%	
SPT	MHA	LoRA matrix decomposition and multi-head feature transformation	sgemm_128x64_tn	13.5 ms	61.9%
		Multi-head attention calculation	cusparse::sddmm_ker	1.8 ms	8.4%
			cusparse::csrmm_alg2	1.7 ms	8.0%
			pq_lookup_kernel	1.1 ms	5.0%
	FFN	LoRA matrix decomposition and feedforward feature transformation	sgemm_128x64_tn	7.1 ms	48.4%
			sgemm_128x64_nn	6.9 ms	47.1%
		Index select or put operators	index_put_kernel	1.0 ms	6.8%
			index_get_kernel	0.4 ms	2.7%
Reshape, addition, or activation operators		elementwise_kernel	0.7 ms	4.8%	

time complexity compared to vanilla MHA as shown in §4.1, but provides limited speedup on GPUs. This is because modern GPUs are optimized for contiguous memory access patterns, while sparse attention involves more irregular memory accesses, which limit the actual speedup gained.

Second, our routed FFN effectively reduces the running time compared with vanilla FFN. This is accomplished by the routed FFN reducing the number of parameters activated per token. Additionally, Table 4 demonstrates that the speedup achieved by the routed FFN is near the theoretical maximum, i.e., achieving 2.0x and 1.3x speedups with non-zero portions of 1/2 and 3/4, indicating our implementations utilize computational resources efficiently. The peak memory reduction brought by routed FFN is less significant because the sizes of the input, output, and weight tensors remain unchanged. Moreover, compiled LoRA yields limited gain over LoRA in both time and memory. This is because the baseline has already been highly optimized, with most of the time spent on basic matrix calculations that are difficult to optimize further. This shows that it is necessary to conduct tailored algorithm and system optimizations for Transformer as in our work.

Kernel breakdown. In Table 5, we break the running time of our sparse MHA and routed FFN into their constituting GPU kernels and compare them with the vanilla counterparts. The Transformer block is OPT-2048, and we consider only the forward pass for simplicity. We make the following observations from the results.

First, peak memory reduction is the priority for sparse MHA since the LoRA decomposition and multi-head feature transformations inevitably take up most of the compute time, which leaves limited opportunity for speedup. The high overhead of multi-head feature transformation was also observed in other research [32]. Moreover, sparse MHA offers no speedup over dense matrices because dense matrix operators enjoy fast contiguous memory accesses from modern hardware while random memory accesses

Table 6: Compare with an alternative MHA implementation.

Module	Method	Peak Mem	Duration
MHA	SPT	1123 MB	54.1 ms
	Naive-PQ	1253 MB	248.9 ms

occupy a large part of sparse matrix operators. According to these observations, we decide that reducing the memory usage of MHA should take priority over achieving speedup. Second, routed FFN effectively reduces the computation cost of FFN (i.e., which are mainly GEMM operations), and the overhead of the router network is negligible. The dynamically skipped blocks in the routed FFN translate almost directly to an equivalent speedup. The breakdown also shows that our routed FFN introduces `index_put` and `index_get` operators for batching tokens, and their overheads are only 13% of overall running time.

Alternative implementations. In Table 6, we compare our sparse MHA with an alternative implementation, which also uses PQ but adopts the standard practice to compute and sort floating point query-key similarity scores. The Transformer block is OPT-2048, and the experiment settings are the same as Table 4. Table 6 shows that the Naive-PQ implementation has slightly higher memory consumption than our bucket-sort based implementation but its running time is 4.6 \times of our implementation. This is because Naive-PQ suffers from a high complexity in computing and sorting floating point query-key similarity scores, and shows the effectiveness of our implementation.

We also experimented with using the BSR approach as an alternative for our routed FFN, which generates a parameter mask for each token to conduct batched computation. This experiment runs OOM because when the input tokens are the size of [16, 512], the BSR masks take up 200GB, which far exceeds our GPU memory

capacity. In contrast, our routed FFN implementation batches the tokens according to their activated parameter blocks. It does not rely on the masks and achieves a speedup close to theory as shown by Table 6. Implementing the proposed optimizations is critical to enabling SPT and avoiding system failures due to excessive memory and computation demands.

7 RELATED WORK

Large Transformer models, such as BERT [11], RoBERTa [25], GPT-2 [30], OPT [46], LLaMa [40], and ViT [13], achieve tremendous success recently and are used for an increasing number of applications. However, these models are prohibitively expensive to train due to their large sizes, and we discuss the most widely used techniques for training or fine-tuning large Transformer models.

Distributed training. To handle large datasets and models, Transformer training can be parallelized across many GPUs. As the two most common approaches, data parallelism assigns the GPUs to process different training samples by keeping a replica of the model on each GPU, and model parallelism partitions the model over the GPUs and transfers intermediate activation across GPUs [23]. Pipeline parallelism reduces the idle time of model parallelism by pipelining multiple mini-batches [19], and hybrid parallelism flexibly partitions training workload in dimensions such as sample, feature, and model for short training time [21]. Many systems support distributed training. For instance, DeepSpeed [31] and Megatron-LM [28] optimize pipelining and scheduling across multiple GPUs for training throughput. PyTorch introduces fully sharded data parallelism (FSDP) [49] to simplify distributed training for large Transformers. Our work is largely orthogonal to these distributed training works, and the only consideration is that when the distribution strategy partitions computations intra-layer, the mentioned operators in §5 would need distributed implementations.

Accelerate Transformers. Some works conduct fine-grained CPU or GPU optimizations for Transformer execution. FasterTransformer and FlashAttention [8] implement hand-crafted GPU kernels to minimize data transfer and reuse data in cache. TurboTransformers [14] shows that reduced memory footprint and better memory management can reduce the running time of Transformer models. Triton [38] is utilized by PyTorch as a compiler to optimize the computation graphs of neural networks, it achieves comparable performance to hand-tuned kernels, which served as part of our baselines for evaluating time and memory costs in §6.3. Model quantization converts the floating point model weights to lower precision to improve efficiency but model quality is usually sacrificed [9, 10]. Our GPU kernel optimizations target the sparse MHA and routed FFN and thus are different from these works, and we could also benefit from using low-precision model weights.

Fine-tuning Transformers. Adapter-based methods are widely used to fine-tune Transformers for downstream tasks [5, 17]. They freeze the parameters of the pre-trained model to preserve the learned knowledge and introduce a small number of trainable parameters to adapt to the specific task. In particular, BitFit [44] only fine-tunes the bias vectors in a pre-trained model. Input-Tuning [1] introduces adapters in the input embedding layers to process contexts. LoRA [10] adds low-rank matrices to all layers and yields

competitive model quality to full tuning. Transformer is also widely used by computer vision models recently [13]. A popular approach to fine-tune vision Transformers is called ControlNet [45], which adds convolution control networks to a pre-trained model. Our work improves LoRA, the state-of-the-art fine-tuning method for Transformer-based language models, and may also benefit Transformers in computer vision models.

Transformer variants. It has been observed that the output of the softmax function is dominated by a few top entries for classification models [26, 47, 48]. Our sparse MHA is driven by similar observation but tackles the challenge of efficiently identifying the top- L query-key pairs. To process longer sequences, ReFormer [22] replaces the inner product attention with locality sensitive hashing (LSH) attention, and Recurrent Memory Transformer [3] uses an additional external memory module to store long-term context. Mixture-of-Experts (MoE) [33] and Switch Transformer [15] introduce sparsely activated weight for Transformers by modifying the FFN module to improve model capacity. Some of these works share the idea of utilizing sparsity with our work but their purposes are different, e.g., process longer sequence and increase model capacity. Moreover, they are required to train the models from scratch using their Transformer architectures while we focus on fine-tuning pre-trained models.

8 CONCLUSIONS

In this paper, we present the SPT system for the efficient fine-tuning of Transformer-based large language models. We observe that the main memory consumption of Transformer is used to store the attention weights for multi-head attention (MHA) and the majority of running time is spent on the feed-forward network (FFN). From the algorithm perspective, we propose the sparse MHA and routed FFN modules to expose sparsity for reduced memory consumption and running time. From the system perspective, we customize CUDA implementations for sparse MHA and routed FFN to conduct sparse training efficiently on GPU. Experiment results show that SPT effectively both reduces training time and memory consumption.

REFERENCES

- [1] Shengnan An, Yifei Li, Zeqi Lin, Qian Liu, Bei Chen, Qiang Fu, Weizhu Chen, Nanning Zheng, and Jian-Guang Lou. 2022. Input-Tuning: Adapting Unfamiliar Inputs to Frozen Pretrained Models. *CoRR* abs/2203.03131 (2022). <https://doi.org/10.48550/ARXIV.2203.03131> arXiv:2203.03131
- [2] Iz Beltagy, Matthew E. Peters, and Arman Cohan. 2020. Longformer: The Long-Document Transformer. *arXiv:2004.05150* (2020).
- [3] Aydar Bulatov, Yuri Kuratov, and Mikhail S. Burtsev. 2022. Recurrent Memory Transformer. *CoRR* abs/2207.06881 (2022). <https://doi.org/10.48550/arXiv.2207.06881> arXiv:2207.06881
- [4] Shoufa Chen, Chongjian Ge, Zhan Tong, Jiangliu Wang, Yibing Song, Jue Wang, and Ping Luo. 2022. Adaptformer: Adapting vision transformers for scalable visual recognition. *Advances in Neural Information Processing Systems* 35 (2022), 16664–16678.
- [5] Zhe Chen, Yuchen Duan, Wenhai Wang, Junjun He, Tong Lu, Jifeng Dai, and Yu Qiao. 2022. Vision Transformer Adapter for Dense Predictions. *CoRR* abs/2205.08534 (2022). <https://doi.org/10.48550/arXiv.2205.08534> arXiv:2205.08534
- [6] Minsik Cho, Keivan Alizadeh-Vahid, Saurabh Adya, and Mohammad Rastegari. 2022. DKM: Differentiable k-Means Clustering Layer for Neural Network Compression. In *The Tenth International Conference on Learning Representations, ICLR 2022, Virtual Event, April 25–29, 2022*. OpenReview.net. https://openreview.net/forum?id=J_F_qqCE3Z5

- [7] Aakanksha Chowdhery, Sharan Narang, Jacob Devlin, Maarten Bosma, Gaurav Mishra, Adam Roberts, Paul Barham, Hyung Won Chung, Charles Sutton, Sebastian Gehrmann, Parker Schuh, Kensen Shi, Sasha Tsvyashchenko, Joshua Maynez, Abhishek Rao, Parker Barnes, Yi Tay, Noam Shazeer, Vinodkumar Prabhakaran, Emily Reif, Nan Du, Ben Hutchinson, Reiner Pope, James Bradbury, Jacob Austin, Michael Isard, Guy Gur-Ari, Pengcheng Yin, Toju Duke, Anselm Levskaya, Sanjay Ghemawat, Sunipa Dev, Henryk Michalewski, Xavier Garcia, Vedant Misra, Kevin Robinson, Liam Fedus, Denny Zhou, Daphne Ip-polito, David Luan, Hyeontaek Lim, Barret Zoph, Alexander Spiridonov, Ryan Sepassi, David Dohan, Shivani Agrawal, Mark Omernick, Andrew M. Dai, Thanu-malayan Sankaranarayanan Pillai, Marie Pellat, Aitor Lewkowycz, Erica Moreira, Rewon Child, Oleksandr Polozov, Katherine Lee, Zongwei Zhou, Xuezhi Wang, Brennan Saeta, Mark Diaz, Orhan Firat, Michele Catasta, Jason Wei, Kathy Meier-Hellstern, Douglas Eck, Jeff Dean, Slav Petrov, and Noah Fiedel. 2023. PaLM: Scaling Language Modeling with Pathways. *J. Mach. Learn. Res.* 24 (2023), 240:1–240:113. <http://jmlr.org/papers/v24/22-1144.html>
- [8] Tri Dao, Daniel Y. Fu, Stefano Ermon, Atri Rudra, and Christopher Ré. 2022. FlashAttention: Fast and Memory-Efficient Exact Attention with IO-Awareness. In *NeurIPS*. http://papers.nips.cc/paper_files/paper/2022/hash/67d57c32e20fd0a7a302cb81d36e40d5-Abstract-Conference.html
- [9] Tim Dettmers, Mike Lewis, Younes Belkada, and Luke Zettlemoyer. 2022. LLM.int8(): 8-bit Matrix Multiplication for Transformers at Scale. *CoRR abs/2208.07339* (2022). <https://doi.org/10.48550/ARXIV.2208.07339> arXiv:2208.07339
- [10] Tim Dettmers, Artidoro Pagnoni, Ari Holtzman, and Luke Zettlemoyer. 2023. QLoRA: Efficient Finetuning of Quantized LLMs. *CoRR abs/2305.14314* (2023). <https://doi.org/10.48550/ARXIV.2305.14314> arXiv:2305.14314
- [11] Jacob Devlin, Ming-Wei Chang, Kenton Lee, and Kristina Toutanova. 2018. BERT: Pre-training of Deep Bidirectional Transformers for Language Understanding. *CoRR abs/1810.04805* (2018). arXiv:1810.04805 <http://arxiv.org/abs/1810.04805>
- [12] Ning Ding, Yujia Qin, Guang Yang, Fuchao Wei, Zonghan Yang, Yusheng Su, Shengding Hu, Yulin Chen, Chi-Min Chan, Weize Chen, Jing Yi, Weilin Zhao, Xiaozhi Wang, Zhiyuan Liu, Hai-Tao Zheng, Jianfei Chen, Yang Liu, Jie Tang, Juanzi Li, and Maosong Sun. 2022. Delta Tuning: A Comprehensive Study of Parameter Efficient Methods for Pre-trained Language Models. arXiv:2203.06904 [cs.CL]
- [13] Alexey Dosovitskiy, Lucas Beyer, Alexander Kolesnikov, Dirk Weissenborn, Xi-aohua Zhai, Thomas Unterthiner, Mostafa Dehghani, Matthias Minderer, Georg Heigold, Sylvain Gelly, Jakob Uszkoreit, and Neil Houlsby. 2021. An Image is Worth 16x16 Words: Transformers for Image Recognition at Scale. In *9th International Conference on Learning Representations, ICLR 2021, Virtual Event, Austria, May 3-7, 2021*. OpenReview.net. <https://openreview.net/forum?id=YicbFdNTTy>
- [14] Jiarui Fang, Yang Yu, Chengduo Zhao, and Jie Zhou. 2021. TurboTransformers: an efficient GPU serving system for transformer models. In *PPoPP '21: 26th ACM SIGPLAN Symposium on Principles and Practice of Parallel Programming, Virtual Event, Republic of Korea, February 27- March 3, 2021*, Jaejin Lee and Erez Petrank (Eds.). ACM, 389–402. <https://doi.org/10.1145/3437801.3441578>
- [15] William Fedus, Barret Zoph, and Noam Shazeer. 2022. Switch Transformers: Scaling to Trillion Parameter Models with Simple and Efficient Sparsity. *J. Mach. Learn. Res.* 23 (2022), 120:1–120:39. <http://jmlr.org/papers/v23/21-0998.html>
- [16] Dan Hendrycks, Collin Burns, Steven Basart, Andy Zou, Mantas Mazeika, Dawn Song, and Jacob Steinhardt. 2021. Measuring Massive Multitask Language Understanding. In *9th International Conference on Learning Representations, ICLR 2021, Virtual Event, Austria, May 3-7, 2021*. OpenReview.net. <https://openreview.net/forum?id=d7KBjml3GmQ>
- [17] Neil Houlsby, Andrei Giurgiu, Stanislaw Jastrzebski, Bruna Morrone, Quentin de Laroussilhe, Andrea Gesmundo, Mona Attariyan, and Sylvain Gelly. 2019. Parameter-Efficient Transfer Learning for NLP. In *Proceedings of the 36th International Conference on Machine Learning, ICML 2019, 9-15 June 2019, Long Beach, California, USA (Proceedings of Machine Learning Research, Vol. 97)*, Kamalika Chaudhuri and Ruslan Salakhutdinov (Eds.). PMLR, 2790–2799. <http://proceedings.mlr.press/v97/houlsby19a.html>
- [18] Edward J. Hu, Yelong Shen, Phillip Wallis, Zeyuan Allen-Zhu, Yuanzhi Li, Shean Wang, Lu Wang, and Weizhu Chen. 2022. LoRA: Low-Rank Adaptation of Large Language Models. In *The Tenth International Conference on Learning Representations, ICLR 2022, Virtual Event, April 25-29, 2022*. OpenReview.net. <https://openreview.net/forum?id=aZeVKeeFYf9>
- [19] Yanping Huang, Youlong Cheng, Ankur Bapna, Orhan Firat, Dehao Chen, Mia Xu Chen, HyoukJoong Lee, Jiquan Ngiam, Quoc V. Le, Yonghui Wu, and Zhiheng Chen. 2019. GPipe: Efficient Training of Giant Neural Networks using Pipeline Parallelism. In *Advances in Neural Information Processing Systems 32: Annual Conference on Neural Information Processing Systems 2019, NeurIPS 2019, December 8-14, 2019, Vancouver, BC, Canada*, Hanna M. Wallach, Hugo Larochelle, Alina Beygelzimer, Florence d'Alché-Buc, Emily B. Fox, and Roman Garnett (Eds.), 103–112. <https://proceedings.neurips.cc/paper/2019/hash/093f65e080a295f8076b1c5722a46aa2-Abstract.html>
- [20] Jeff Johnson, Matthijs Douze, and Hervé Jégou. 2019. Billion-scale similarity search with GPUs. *IEEE Transactions on Big Data* 7, 3 (2019), 535–547.
- [21] Soojeong Kim, Gyeong-In Yu, Hojin Park, Sungwoo Cho, Eunji Jeong, Hyeonmin Ha, Sanha Lee, Joo Seong Jeong, and Byung-Gon Chun. 2019. Parallax: Sparsity-aware Data Parallel Training of Deep Neural Networks. In *Proceedings of the Fourteenth EuroSys Conference 2019, Dresden, Germany, March 25-28, 2019*, George Candea, Robert van Renesse, and Christof Fetzer (Eds.). ACM, 43:1–43:15. <https://doi.org/10.1145/3302424.3303957>
- [22] Nikita Kitaev, Lukasz Kaiser, and Anselm Levskaya. 2020. Reformer: The Efficient Transformer. In *8th International Conference on Learning Representations, ICLR 2020, Addis Ababa, Ethiopia, April 26-30, 2020*. OpenReview.net. <https://openreview.net/forum?id=rkgNKKHtvB>
- [23] Shen Li, Yanli Zhao, Rohan Varma, Omkar Salpekar, Pieter Noordhuis, Teng Li, Adam Paszke, Jeff Smith, Brian Vaughan, Pritam Damania, and Soumith Chintala. 2020. PyTorch Distributed: Experiences on Accelerating Data Parallel Training. *Proc. VLDB Endow.* 13, 12 (2020), 3005–3018. <https://doi.org/10.14778/3415478.3415530>
- [24] Haokun Liu, Derek Tam, Mohammed Muqeeth, Jay Mohta, Tenghao Huang, Mohit Bansal, and Colin A Raffel. 2022. Few-Shot Parameter-Efficient Fine-Tuning is Better and Cheaper than In-Context Learning. In *Advances in Neural Information Processing Systems*, S. Koyejo, S. Mohamed, A. Agarwal, D. Belgrave, K. Cho, and A. Oh (Eds.), Vol. 35. Curran Associates, Inc., 1950–1965. https://proceedings.neurips.cc/paper_files/paper/2022/file/0cde695b83bd186c1fd456302888454c-Paper-Conference.pdf
- [25] Yinhan Liu, Myle Ott, Naman Goyal, Jingfei Du, Mandar Joshi, Danqi Chen, Omer Levy, Mike Lewis, Luke Zettlemoyer, and Veselin Stoyanov. 2019. RoBERTa: A Robustly Optimized BERT Pretraining Approach. *CoRR abs/1907.11692* (2019). arXiv:1907.11692 <http://arxiv.org/abs/1907.11692>
- [26] Andre Martins and Ramon Astudillo. 2016. From Softmax to Sparsemax: A Sparse Model of Attention and Multi-Label Classification. In *Proceedings of the 33rd International Conference on Machine Learning (Proceedings of Machine Learning Research, Vol. 48)*, Maria Florina Balcan and Kilian Q. Weinberger (Eds.). PMLR, New York, New York, USA, 1614–1623. <https://proceedings.mlr.press/v48/martins16.html>
- [27] Stephen Merity, Caiming Xiong, James Bradbury, and Richard Socher. 2016. Pointer Sentinel Mixture Models. arXiv:1609.07843 [cs.CL]
- [28] Deepak Narayanan, Mohammad Shoeybi, Jared Casper, Patrick LeGresley, Mostafa Natavary, Vijay Korthikanti, Dmitri Vainbrand, Prithvi Kashinkunti, Julie Bernauer, Bryan Catanzaro, Amar Phanishayee, and Matei Zaharia. 2021. Efficient large-scale language model training on GPU clusters using megatron-LM. In *International Conference for High Performance Computing, Networking, Storage and Analysis, SC 2021, St. Louis, Missouri, USA, November 14-19, 2021*, Bronis R. de Supinski, Mary W. Hall, and Todd Gamblin (Eds.). ACM, 58. <https://doi.org/10.1145/3458817.3476209>
- [29] Adam Paszke, Sam Gross, Francisco Massa, Adam Lerer, James Bradbury, Gregory Chanan, Trevor Killeen, Zeming Lin, Natalia Gimelshein, Luca Antiga, Alban Desmaison, Andreas Köpf, Edward Z. Yang, Zachary DeVito, Martin Raison, Alykhan Tejani, Sasank Chilamkurthy, Benoit Steiner, Lu Fang, Junjie Bai, and Soumith Chintala. 2019. PyTorch: An Imperative Style, High-Performance Deep Learning Library. In *Advances in Neural Information Processing Systems 32: Annual Conference on Neural Information Processing Systems 2019, NeurIPS 2019, December 8-14, 2019, Vancouver, BC, Canada*, Hanna M. Wallach, Hugo Larochelle, Alina Beygelzimer, Florence d'Alché-Buc, Emily B. Fox, and Roman Garnett (Eds.), 8024–8035. <https://proceedings.neurips.cc/paper/2019/hash/bdbca288fee7f92f2bfa9f7012727740-Abstract.html>
- [30] Alec Radford, Jeffrey Wu, Rewon Child, David Luan, Dario Amodei, Ilya Sutskever, et al. 2019. Language models are unsupervised multitask learners. *OpenAI blog* 1, 8 (2019), 9.
- [31] Jeff Rasley, Samyam Rajbhandari, Olatunji Ruwase, and Yuxiong He. 2020. DeepSpeed: System Optimizations Enable Training Deep Learning Models with Over 100 Billion Parameters. In *KDD '20: The 26th ACM SIGKDD Conference on Knowledge Discovery and Data Mining, Virtual Event, CA, USA, August 23-27, 2020*, Rajesh Gupta, Yan Liu, Jiliang Tang, and B. Aditya Prakash (Eds.). ACM, 3505–3506. <https://doi.org/10.1145/3394486.3406703>
- [32] Noam Shazeer. 2019. Fast Transformer Decoding: One Write-Head is All You Need. *CoRR abs/1911.02150* (2019). arXiv:1911.02150 <http://arxiv.org/abs/1911.02150>
- [33] Noam Shazeer, Azalia Mirhoseini, Krzysztof Maziarz, Andy Davis, Quoc V. Le, Geoffrey E. Hinton, and Jeff Dean. 2017. Outrageously Large Neural Networks: The Sparsely-Gated Mixture-of-Experts Layer. *CoRR abs/1701.06538* (2017). arXiv:1701.06538 <http://arxiv.org/abs/1701.06538>
- [34] Fumin Shen, Wei Liu, Shaoting Zhang, Yang Yang, and Heng Tao Shen. 2015. Learning Binary Codes for Maximum Inner Product Search. In *2015 IEEE International Conference on Computer Vision, ICCV 2015, Santiago, Chile, December 7-13, 2015*. IEEE Computer Society, 4148–4156. <https://doi.org/10.1109/ICCV.2015.472>
- [35] Jianlin Lu, Yu Lu, Shengfeng Pan, Bo Wen, and Yufeng Liu. 2021. RoFormer: Enhanced Transformer with Rotary Position Embedding. *CoRR abs/2104.09864* (2021). arXiv:2104.09864 <https://arxiv.org/abs/2104.09864>

- [36] Rohan Taori, Ishaan Gulrajani, Tianyi Zhang, Yann Dubois, Xuechen Li, Carlos Guestrin, Percy Liang, and Tatsunori B Hashimoto. 2023. Alpaca: A strong, replicable instruction-following model. *Stanford Center for Research on Foundation Models*. <https://crfm.stanford.edu/2023/03/13/alpaca.html> 3, 6 (2023), 7.
- [37] Rohan Taori, Ishaan Gulrajani, Tianyi Zhang, Yann Dubois, Xuechen Li, Carlos Guestrin, Percy Liang, and Tatsunori B Hashimoto. 2023. Stanford Alpaca: An Instruction-following LLaMA model. https://github.com/tatsu-lab/stanford_alpaca.
- [38] Philippe Tillet, Hsiang-Tsung Kung, and David D. Cox. 2019. Triton: an intermediate language and compiler for tiled neural network computations. In *Proceedings of the 3rd ACM SIGPLAN International Workshop on Machine Learning and Programming Languages, MAPL@PLDI 2019, Phoenix, AZ, USA, June 22, 2019*, Tim Mattson, Abdullah Muzahid, and Armando Solar-Lezama (Eds.). ACM, 10–19. <https://doi.org/10.1145/3315508.3329973>
- [39] Mo Tiwari, Ryan Kang, Je-Yong Lee, Luke Lee, Chris Piech, Sebastian Thrun, Ilan Shomorony, and Martin Jinye Zhang. 2022. Faster Maximum Inner Product Search in High Dimensions. *CoRR abs/2212.07551* (2022). <https://doi.org/10.48550/ARXIV.2212.07551> arXiv:2212.07551
- [40] Hugo Touvron, Thibaut Lavril, Gautier Izacard, Xavier Martinet, Marie-Anne Lachaux, Timothée Lacroix, Baptiste Rozière, Naman Goyal, Eric Hambro, Faisal Azhar, Aurélien Rodriguez, Armand Joulin, Edouard Grave, and Guillaume Lample. 2023. LLaMA: Open and Efficient Foundation Language Models. *CoRR abs/2302.13971* (2023). <https://doi.org/10.48550/ARXIV.2302.13971> arXiv:2302.13971
- [41] Hugo Touvron, Louis Martin, Kevin Stone, Peter Albert, Amjad Almahairi, Yasmine Babaei, Nikolay Bashlykov, Soumya Batra, Prajwal Bhargava, Shruti Bhosale, et al. 2023. Llama 2: Open Foundation and Fine-Tuned Chat Models. *arXiv preprint arXiv:2307.09288* (2023).
- [42] Yulong Wang, Xiaolu Zhang, Xiaolin Hu, Bo Zhang, and Hang Su. 2020. Dynamic Network Pruning with Interpretable Layerwise Channel Selection. In *The Thirty-Fourth AAAI Conference on Artificial Intelligence, AAAI 2020, The Thirty-Second Innovative Applications of Artificial Intelligence Conference, IAAI 2020, The Tenth AAAI Symposium on Educational Advances in Artificial Intelligence, EAAI 2020, New York, NY, USA, February 7-12, 2020*. AAAI Press, 6299–6306. <https://doi.org/10.1609/aaai.v34i04.6098>
- [43] Mengzhou Xia and Tianyu Gao. 2023. Sheared LLaMA: Accelerating Language Model Pre-training via Structured Pruning. (2023).
- [44] Elad Ben Zaken, Yoav Goldberg, and Shauli Ravfogel. 2022. BitFit: Simple Parameter-efficient Fine-tuning for Transformer-based Masked Language-models. In *Proceedings of the 60th Annual Meeting of the Association for Computational Linguistics (Volume 2: Short Papers), ACL 2022, Dublin, Ireland, May 22-27, 2022*, Smaranda Muresan, Preslav Nakov, and Aline Villavicencio (Eds.). Association for Computational Linguistics, 1–9. <https://doi.org/10.18653/V1/2022.ACL-SHORT.1>
- [45] Lvmin Zhang and Maneesh Agrawala. 2023. Adding conditional control to text-to-image diffusion models. *arXiv preprint arXiv:2302.05543* (2023).
- [46] Susan Zhang, Stephen Roller, Naman Goyal, Mikel Artetxe, Moya Chen, Shuohui Chen, Christopher Dewan, Mona T. Diab, Xian Li, Xi Victoria Lin, Todor Mihaylov, Myle Ott, Sam Shleifer, Kurt Shuster, Daniel Simig, Punit Singh Koura, Anjali Sridhar, Tianlu Wang, and Luke Zettlemoyer. 2022. OPT: Open Pre-trained Transformer Language Models. *CoRR abs/2205.01068* (2022). <https://doi.org/10.48550/ARXIV.2205.01068> arXiv:2205.01068
- [47] Xingcheng Zhang, Lei Yang, Junjie Yan, and Dahua Lin. 2018. Accelerated Training for Massive Classification via Dynamic Class Selection. In *Proceedings of the Thirty-Second AAAI Conference on Artificial Intelligence, (AAAI-18), the 30th innovative Applications of Artificial Intelligence (IAAI-18), and the 8th AAAI Symposium on Educational Advances in Artificial Intelligence (EAAI-18), New Orleans, Louisiana, USA, February 2-7, 2018*, Sheila A. McIlraith and Kilian Q. Weinberger (Eds.). AAAI Press, 7566–7573. <https://doi.org/10.1609/AAAI.V32I1.12337>
- [48] Kang Zhao, Liuyihan Song, Yingya Zhang, Pan Pan, Yinghui Xu, and Rong Jin. 2021. ANN Softmax: Acceleration of Extreme Classification Training. *Proc. VLDB Endow.* 15, 1 (2021), 1–10. <https://doi.org/10.14778/3485450.3485451>
- [49] Yanli Zhao, Andrew Gu, Rohan Varma, Liang Luo, Chien-Chin Huang, Min Xu, Less Wright, Hamid Shojanazeri, Myle Ott, Sam Shleifer, Alban Desmaison, Can Balioglu, Bernard Nguyen, Geeta Chauhan, Yuchen Hao, and Shen Li. 2023. PyTorch FSDP: Experiences on Scaling Fully Sharded Data Parallel. *CoRR abs/2304.11277* (2023). <https://doi.org/10.48550/arXiv.2304.11277> arXiv:2304.11277

A ARTIFACT AND REPRODUCIBILITY

This appendix provides detailed guidance on replicating the most significant experimental outcomes obtained by SPT. In §A.1, we present the experimental setup. We then show three main topics: correctness (§A.2), efficiency (§A.3), and model quality (§A.4).

A.1 Experiment Setup

Preparation procedures for the experiments.

Hardware. This experiment is configured to be runnable on a single NVIDIA RTX 3090 (24GB memory) GPU. We also tested RTX 2080 TI (11 GB memory). Other GPU models may work, but have not been fully validated.

Software. The required softwares are listed in Table 7.

Table 7: Software versions.

name	version
Ubuntu	18.04 or above
Kernel	4.15.0-175 or above
GCC	7.5.0 or above
GPU-Driver	465.19.01 or above
CUDA-Toolkit	11.8, minimum 11.0
Python	3.10.7 or above
PyTorch	2.0.1 or above

Build Essentials. *build-essential*, *python3-setuptools*, and *ninja-build* are required.

Installing CUDA. Download and install CUDA 11.8 and compatible drivers³.

Installing Conda. Install Anaconda or Miniconda⁴.

Creating Python Environment. Create a new clean environment with “*conda create -n spt python=3.10 && source activate spt*”

Installing dependencies. The following packages are required:

- PyTorch Basic: *pip3 install torch==2.0.1 torchedata transformers*
- End-to-end: *pip3 install lightning==2.0.8 deepspeed torchmetrics*

Note that here we use *pip3* to install packages inside the virtual environment, *conda* can also be used here, but some package names may differ between *pip* and *conda*.

A.2 Correctness

Correctness is the most fundamental prerequisite for the whole implementation. We ensure SPT works as expected by performing extensive unit tests. Here we list 7 main unit tests,

- *test_cdist.py*: checking CUDA kernel results on fused collection distance calculation kernel (*cdist* in §5.1) with unfused PyTorch implementation.
- *test_lookup.py*: checking CUDA kernel results of the bucket sort shown in §5.1, this ensures that SPT retrieved the query-key vectors correctly.

```
def test_softmax():
    # y_1, grad_1: torch kernel
    y_1 = torch.softmax(dense, dim=-1)
    torch.max(y_1).backward()
    grad_1 = dense.grad.detach().clone()

    # y_2, grad_2: custom kernel
    y_2 = kernels.softmax(
        indptr, indices, values
    )
    torch.max(y_2).backward()
    grad_2 = values.grad.detach().clone()

    # check results
    assert torch.allclose(y_1, y_2.to_dense(), atol=1e-2)
    assert torch.allclose(grad_1, grad_2.to_dense(), atol=1e-2)
```

Figure 11: A sample unittest to check both forward and backward passes of an operator.

- *test_sddmm.py* and *test_spmv.py*: checking sparse matrix multiplications with equivalent dense matrix computations, this also ensures the *Indptr* and *Indices* shown in §5.1 are well constructed.
- *test_softmax.py*: checking CUDA kernel results on sparse matrices. Note that softmax is numerically sensitive, a tiny *error* ≤ 0.01 is allowed in the unit test.
- *test_sparse_mha.py* and *test_routed_ffn.py*: checking the correctness of the proposed sparse MHA and routed MHA by comparing results with naive and not optimized implementations.

Note that both forward pass and backward pass results are carefully verified, Figure 11 shows a sample unittest test to make sure the customized operators computes correct output and gradient.

A.3 Efficiency

We provide a python script *script/profile.py* to easily profile the main modules of SPT, different Transformer configurations and fine-tuning methods can be set. The script takes 8 arguments:

- *-name* (required): specifying the Transformer configuration to use, can be one of *opt-1024*, *opt-2048*, *opt-2560*, *llama-2560*, or *llama-4096*.
- *-tuning* (required): choosing the fine-tuning method to evaluate, which can be *full*, *lora*, or *sparse*.
- *-module* (required): specifying the module to evaluate, can be one of *mha*, *ffn*, or *both*.
- *-d_lora* (default 16): specifying the low-rank decomposition dimension of LoRA, which is ignored for full-parameter tuning.
- *-seq_length* (default 512) and *-batch_size* (default 16): specifying the sequence length and batch size.
- *-backward*: choosing whether or not to profile on backward passes.
- *-compile*: choosing whether or not to enable *torch.compile*.

Specifically, SPT can be reproduced by running: *python3 script/profile.py -name='opt-2048' -tuning='sparse' -module='both'*.

The output is printed into the *stdout* stream, which includes all the important metrics and statistics. Figure 12 shows a sample profiling output. Specifically, system configurations, kernel time consumption, and memory statistics are printed in sequence. Note

³<https://developer.nvidia.com/cuda-downloads>

⁴<https://docs.conda.io/projects/miniconda/en/latest/>

```

# logs by our Model Adapter
[UPGRADE] mha.linear_q Linear -> LoRALinear
[UPGRADE] mha.linear_k Linear -> LoRALinear
[UPGRADE] mha.linear_v Linear -> LoRALinear
[UPGRADE] mha.linear_o Linear -> LoRALinear
[UPGRADE] ffd.fc1 Linear -> LoRALinear
[UPGRADE] ffd.fc2 Linear -> LoRALinear

# breakdown and timing (20 runs)
-----
Name          Self CUDA   Self CUDA %   CUDA total
-----
ampere_sgemm_64x64_tn      1.216s      37.55%      1.216s
ampere_sgemm_128x32_nn     624.253ms   19.27%      624.253ms
ampere_sgemm_128x64_tn     290.456ms   8.97%       290.456ms
ampere_sgemm_64x64_nn     267.770ms   8.27%       267.770ms
Memcpy DtoD (Device -> Device) 109.602ms   3.38%       109.602ms
-----
Self CPU time total: 3.004s

# peak memory statistics
=====
|
| PyTorch CUDA memory summary, device ID 0
|-----
| CUDA OOMs: 0 | cudaMalloc retries: 0 | | | |
|---|---|---|---|---|
| Metric      | Cur Usage | Peak Usage | Tot Alloc | Tot Freed |
|-----
| Allocated memory | 416936 KiB | 2714 MiB | 449859 MiB | 449452 MiB |
| from large pool | 409856 KiB | 2704 MiB | 449168 MiB | 448768 MiB |
| from small pool | 7080 KiB | 11 MiB | 691 MiB | 684 MiB |
|-----

```

Figure 12: A sample output of the profile script.

that memory statistics are generated on top of PyTorch’s buffer pool, thus there may be subtle differences under different GPU driver and PyTorch version.

A.4 Model Quality

In this section, we present approaches for assessing the model quality fine-tuned by SPT from two perspectives. Firstly, we evaluate the MMLU score by loading our fine-tuned parameters. Secondly, we provide an end-to-end script that replicates the training procedures.

Table 8: Required checkpoints.

model	file	size	checksum
OPT-125M	opt-125m.ckpt	642 MB	274e1ea1
	opt-125m-spt.ckpt	17 MB	77a96766
OPT-2.7B	opt-2.7b.ckpt	10622 MB	05d331f6
	opt-2.7b-spt.ckpt	100 MB	d6d5c56b
LLaMA-2.7B	sheared-llama-2.7b.ckpt	10434 MB	8cac7a74
	sheared-llama-2.7b-spt.ckpt	102 MB	67f00f2c

MMLU evaluation. We offer three checkpoints (shown in Table 8, checksum is the leading 8 hexdigest of *sha256sum*) for the fine-tuned model, which validate the quality of the reported results. The MMLU evaluation pipeline operates as follows:

- Loading pre-trained model weights from the HuggingFace⁵ model hub and converting them to PyTorch format: `python3 script/profile.py --name='facebook/opt-2.7b'`.

- Loading our fine-tuned weights (the smaller files show in Table 8) that patch onto the pre-trained weights, and evaluating the MMLU score: `python3 script/mmlu-evaluate.py --ckpt='opt-2.7b.ckpt' --spt_ckpt='opt-2.7b-spt.ckpt'`.

This script only evaluates MMLU on 64 samples by default, which can be set to higher via `-test_batches=1024`.

End-to-end fine-tuning. Additionally, we provide end-to-end fine-tuning scripts to replicate the model fine-tuning process. The `sparse-tuning-0.py` script is configured to utilize a single GPU and train the smallest 125M model. On the other hand, `sparse-tuning-1.py` leverages deepspeed for distributed capabilities and requires 4 GPUs. The novel modules mentioned in this work are all pluggable. By customizing the given scripts, models can be fine-tuned while retaining only sparse MHA or routed FFN module.

⁵<https://huggingface.co/facebook/opt-125m>, <https://huggingface.co/facebook/opt-2.7b>, <https://huggingface.co/princeton-nlp/Sheared-LLaMA-2.7B>